



Modeling of cardiac muscle thin films: Pre-stretch, passive and active behavior

Jongmin Shim^{a,*}, Anna Grosberg^b, Janna C. Nawroth^c, Kevin Kit Parker^b, Katia Bertoldi^{a,*}

^a School of Engineering and Applied Science, Harvard University, Cambridge, MA, United States

^b Disease Biophysics Group, Wyss Institute for Biologically Inspired Engineering, School of Engineering and Applied Science, Harvard University, Cambridge, MA, United States

^c Division of Biology, California Institute of Technology, Pasadena, CA, United States

ARTICLE INFO

Article history:

Accepted 4 October 2011

Keywords:

Cardiomyocytes
Cell alignment
Bio-hybrid thin film
Constitutive model
Finite element simulation
Pre-stretch
Isometric twitch stress

ABSTRACT

Recent progress in tissue engineering has made it possible to build contractile bio-hybrid materials that undergo conformational changes by growing a layer of cardiac muscle on elastic polymeric membranes. Further development of such muscular thin films for building actuators and powering devices requires exploring several design parameters, which include the alignment of the cardiac myocytes and the thickness/Young's modulus of elastomeric film. To more efficiently explore these design parameters, we propose a 3-D phenomenological constitutive model, which accounts for both the passive deformation including pre-stretch and the active behavior of the cardiomyocytes. The proposed 3-D constitutive model is implemented within a finite element framework, and can be used to improve the current design of bio-hybrid thin films and help developing bio-hybrid constructs capable of complex conformational changes.

© 2011 Elsevier Ltd. All rights reserved.

1. Introduction

The field of tissue engineering is rapidly moving toward rebuilding living tissues and organs through the development of stem-cell-derived cells and *in vitro* manufacturing of extracellular matrix proteins (Place et al., 2009). Organs and tissues adopt complex 3-D configurations and dynamics, so the capability to model the conformation of engineered tissues is essential for their design. Contractile bio-hybrid materials have been built by growing a monolayer of spatially aligned cardiac myocytes on synthetic elastomeric thin films (Feinberg et al., 2007). When the bio-hybrid film is released into solution and electrically stimulated, the myocytes contract, forcing the construct into adopting a 3-D conformation (Feinberg et al., 2007; Alford et al., 2010). The development of such muscular thin films (MTFs, *i.e.*, a rectangular construct actuated by aligned cardiomyocytes) for building actuators and powering devices requires exploring several design parameters which include the arrangement of the cardiac myocytes and the thickness and Young's modulus of the elastomeric film.

Finite element (FE) analysis provides an efficient way to explore those design parameters, and it will allow researchers to create contractile constructs with non-trivial 3-D geometries (*e.g.*, flexible pumps). Such modeling capability could play an

important role in designing constructs that would finish their building process, or self-assembly *in vivo*. Additionally, it could greatly aid in the development of *in vitro* assays to test pharmaceutical agents for efficacy and toxicity as well as evaluation of stem-cell-derived tissues. For example, a completed FE model which includes fluid-MTF coupling would allow quantification of the resistance experienced by the films at different field frequency and more accurate evaluation of the effect of chronotropic drugs.

Along with the advances in tissue engineering, constitutive models have been proposed to investigate the behavior of anisotropic bio-materials (Spencer, 1984; Weiss et al., 1996) and skeletal muscle (Blemker et al., 2005; Böl and Reese, 2008; Calvo et al., 2010). Cardiac muscle is, like skeletal muscle, characterized by highly organized striated myofibrils; however, it also exhibits spontaneous activity as well as mechanical, chemical, and electrical cell-to-cell coupling (functional syncytium) leading to through-conduction of impulses and, subsequently, a highly synchronous response. Recently, a few researchers (Sainte-Marie et al., 2006; Sermesant et al., 2006; Chapelle et al., 2010) proposed physiology-based models for cardiomyocytes, which considers the mechanism of the involuntary contractile behavior of cardiac muscle due to the action potential under calcium flux and captures the characteristic energy dissipative process of the cardiomyocyte active contribution. However, those physiology-based models are mathematically complex and the identification of the model parameters is very challenging. To overcome these difficulties, Böl et al. (2009) proposed a phenomenological model, which neglects the energy dissipation of the active contribution,

* Corresponding authors.

E-mail addresses: jshim@seas.harvard.edu (J. Shim), bertoldi@seas.harvard.edu (K. Bertoldi).

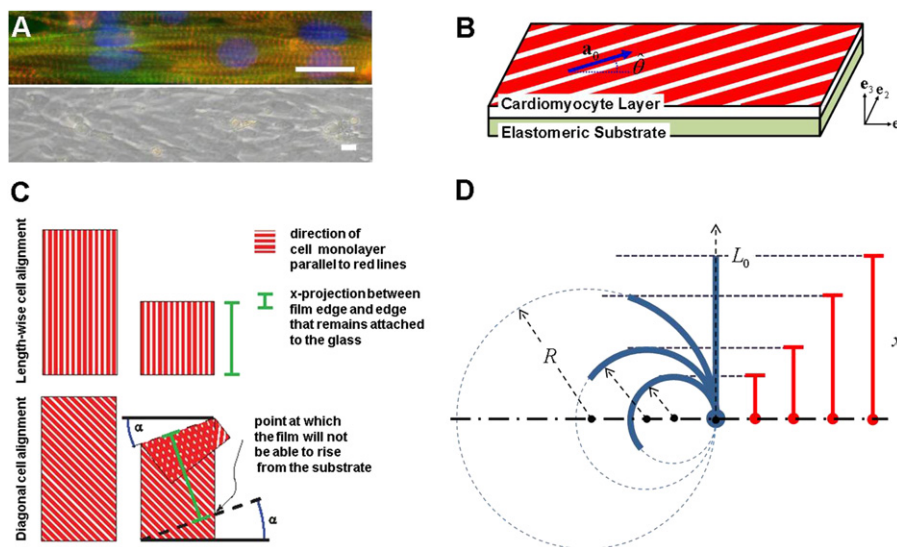


Fig. 1. (A) Top: intracellular alignment of sarcomeres having nuclei (blue), actin (green), alpha-actinin (red). Bottom: a bright-field image of the same tissue showing the overall alignment of cells in the tissue. The length of both scale bars represent 20 μm . (B) Schematic of the muscular thin film (MTF). Here, \mathbf{a}_0 and $\hat{\theta}$ represent the cell alignment vector and the corresponding angle, respectively. (C) Schematic showing the projection of the MTF with length-wise cell alignment (top) and with diagonal cell alignment (bottom). The x-projection is indicated in green and α in blue. (D) Schematic of MTF illustrating the geometric relation of x , L_0 and R in Eq. (1). (For interpretation of the references to color in this figure legend, the reader is referred to the web version of this article.)

leading to a formulation where parameter identification is much easier.

A successful constitutive model of cardiac muscle should capture the active behavior including both systole and diastole and the passive behavior including pre-stretch deformation of the muscle cells¹ and provide an efficient procedure for model parameter identification. Although Böhl et al. (2009) successfully modeled the active behavior of cardiac muscle cells on thin films using 1-D truss-type elements, their model is not able to predict the pre-stretched deformation observed in unconstrained MTFs. Currently there is no phenomenological model capable of capturing all those features. Here, we propose a 3-D phenomenological constitutive model which accounts for both the passive thin film deformation including pre-stretch during cell maturation as well as the active behavior of the cardiac muscle cells. The proposed constitutive model is implemented within a FE framework and used to simulate the experimental results of diastolic and systolic conformations in MTFs. Particularly, in order to accommodate the variation in mechanical properties observed in cultured cardiac tissue, a range of values is identified for both the induced pre-stretch and the isometric twitch stress.

This paper is organized as follows: the experiments for parameter identification and model validation are described in Section 2. In Section 3, the constitutive model is presented for both the elastomeric silicone layer and the cardiac muscle layer. Section 4 demonstrates the model parameter identification results based on literature and experiments with length-wise cell alignment on films. As a validation of the proposed model, Section 5 shows comparison between the numerical and experimental results for constructs with diagonal cell alignment. In addition,

¹ In the following, we will refer to “active” behavior when describing magnitude and time course of stresses and MTF (i.e., a rectangular construct actuated by aligned cardiomyocytes) deformation resulting from cardiomyocytes contraction. These strains and stresses are increasing during the systolic phase until peak systole is reached, and are decreasing during diastole until a fully relaxed state is attained. However, even at this fully relaxed state, MTF curvature might be present due to the pre-stress of the cells, and resulting pre-stretch of the substrate, introduced during tissue maturation. These pre-stresses and strains that are present even at the fully relaxed state will be referred to as “passive” behavior.

parametric studies are also presented to investigate the influence of the thin film thickness, isometric twitch stress, and pre-stretch deformation on MTF conformational changes.

2. Experiments with bio-hybrid films

This section briefly describes the experiments used for identifying parameters and validating the model, and experimental details and methods are provided in Section S1 of the supporting material. Briefly, polydimethylsiloxane (PDMS, Sylgard 184-Dow Corning, Midland, MI) thin films have extracellular matrix proteins, fibronectin patterned on their surface by microcontact printing. Ventricular myocytes from neonatal rats are chemically dissociated and seeded onto the PDMS, where they bind to the fibronectin and self-organize into an anisotropic monolayer whose tissue architecture reflects the orientation of the patterned extracellular matrix (Fig. 1A). The resulting bio-hybrid material is a cantilevered beam anchored to the surface of the two dimensional culture dish (Fig. 1B). During systole, the contracting cell layer would induce a bending deformation in the MTF normal to the plane of the dish (Fig. 1C). To provide the simplest possible deformation geometry to fit the model parameters, the cells were aligned parallel to the MTF length (*length-wise*) (Fig. 1C, top), and the deformation was a simple bending with a constant radius of curvature throughout the MTF. To validate the model with more complex kinematics, we also built chips with *diagonal* alignment of myocytes on the MTF (Fig. 1C, bottom). During the experiments, the MTF’s kinematics was recorded with a high speed camera through a stereomicroscope, and the resultant movies depicted the projection of the films on the substrate plane. The curvature or the radius of curvature were calculated from the projection data and used to quantitatively compare experimental and simulation results (Fig. 1D).

2.1. Experiments for parameter identification and model validation

We tested the contractile response of MTFs with three different PDMS thickness (i.e., 14.5 μm , 18.0 μm , 23.0 μm) for the constructs with length-wise cell alignment and single PDMS

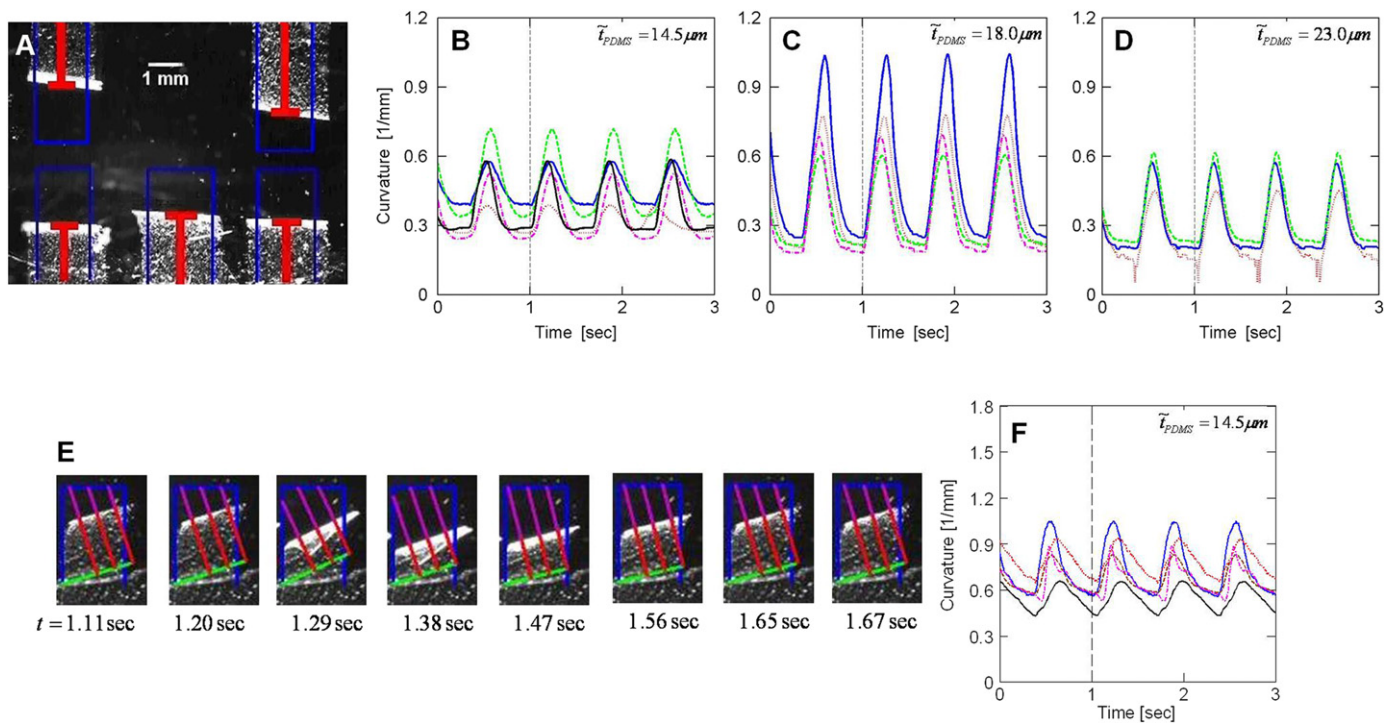


Fig. 2. Experimental results from MTFs with length-wise cell alignment (A–D) and with diagonal cell alignment (E and F). (A) Brightfield image of contractile behavior of MTFs with length-wise cell alignment (PDMS thickness of $14.5\ \mu\text{m}$) taken at $t = 1.215\ \text{s}$. The red line represents the projection length (x in Eq. (1)), and the blue line denotes the original film length (L_0 in Eq. (1)). (B–D) Time–curvature plots for MTFs with length-wise cell alignment. Curvature plots for all films on each chip with three different PDMS thicknesses, i.e., (B) $t_{\text{PDMS}} = 14.5\ \mu\text{m}$, (C) $t_{\text{PDMS}} = 18.0\ \mu\text{m}$, and (D) $t_{\text{PDMS}} = 23.0\ \mu\text{m}$. (E) Snapshots of contractile behavior MTF with diagonal cell alignment (PDMS thickness of $14.5\ \mu\text{m}$). The green line marks the border of the portion of the film lying on glass. The blue line denotes the film when it is completely flat on the glass. The length of the red segment corresponds to x in Eq. (1), while the sum of the lengths of the purple segment and red segment is L_0 in Eq. (1). (F) Time–curvature plots for MTFs with diagonal cell alignment (PDMS thicknesses of $t_{\text{PDMS}} = 14.5\ \mu\text{m}$). (For interpretation of the references to color in this figure legend, the reader is referred to the web version of this article.)

thickness (i.e., $14.5\ \mu\text{m}$) for the constructs with diagonal cell alignment case. Test results for the length-wise cell alignment case are presented in Fig. 2A–D. The experiments were conducted on MTF chips with multiple films on every chip (see Fig. 2A) to replicate the biological variance while constraining engineering variables such as PDMS thickness and cell alignment. The time–curvature plots are presented in Fig. 2B–D. Similarly, Fig. 2E and F summarizes test results from diagonal cell alignment case. Diagonal cell alignment MTFs were also studied on multi-film chips to isolate any biological variations. Indeed, a non-negligible variation of the time–curvature plots under identical experimental conditions can be easily observed. In these experiments, the field stimulated films contracted out of the culture plane as depicted schematically in Fig. 1 and the projection of the MTF tracked with customized software. During diastole, the cells return to their rest length, and the MTF recoils to the rest position. The cyclic bending of the films during $1.5\ \text{Hz}$ stimulation is repeatable and several cardiac cycles worth of data was measured for analysis.

2.2. Data analysis

We assume that the deformed shape of the film is described by the arc of a circle, so that the curvature of the film, K , can be calculated by measuring the projection length x and following the simple relation:

$$x = \begin{cases} R \sin\left(\frac{L_0}{R}\right) & \text{if } x > \frac{L_0}{\pi}, \\ R & \text{if } x \leq \frac{L_0}{\pi}, \end{cases} \quad (1)$$

where $R = 1/K$ is the radius of curvature, and L_0 is the longitudinal length of MTF. The geometric relation of x , L_0 and R is shown in Fig. 1D.

After the experiments were completed the data movies were filtered to remove noise, made binary using image processing software (ImageJ, NIH), and processed using MatLab (Mathworks, Natick, MA) to calculate the curvature of the film. For the case of length-wise cell alignment, the MTF curvature is obtained from the measured projection length, by directly applying Eq. (1). However, with diagonal cell alignment case, due to the non-trivial conformation of the bio-hybrid film, a more elaborated procedure was developed. A parameter, α , is defined as the angle between the film's free and fixed edges (see Fig. 1C (bottom)). We define the base of the film as the line marking the border between the portion of the film lying on the glass and the free section (black dashed line in Fig. 1C). The x -projection length is defined as the distance between the base of the film and the free edge of the film (green solid line in Fig. 1C). Then, the average of temporal MTF curvature (i.e., the prevailing curvature of the MTF) was obtained by minimizing the standard deviation of the temporal curvature collection calculated along the bottom edge of the film. In order to have consistent comparison between the FE model and the experimental results, the movies produced in the simulations and experiments were analyzed using the same software.

3. Constitutive modeling of bio-hybrid films

This section highlights the key components of the proposed constitutive model; its detailed derivation is provided in Section S2 of the supporting material.

Let $\mathbf{F} = \partial \mathbf{x} / \partial \mathbf{X}$ be the deformation gradient mapping a material point from the reference position \mathbf{X} to its current position \mathbf{x} , and $J = \det \mathbf{F}$ be its determinant. The behavior of nearly incompressible materials is effectively described by splitting the deformation locally into volumetric (denoted by superscript ν) and isochoric (denoted by superscript i) components as

$$\mathbf{F} = \mathbf{F}^\nu \cdot \mathbf{F}^i, \quad \text{where } \mathbf{F}^\nu = J^{1/3} \mathbf{1}, \quad \mathbf{F}^i = J^{-1/3} \mathbf{F}. \quad (2)$$

3.1. Elastomeric substrate

The elastomeric substrate is fabricated using PDMS, and its behavior is well captured using a neo-Hookean model. Based on the kinematic assumption shown in Eq. (2) with $\mathbf{C}^i = \mathbf{F}^{iT} \cdot \mathbf{F}^i$ and $\bar{I}_1 = \text{tr} \mathbf{C}^i$, a decoupled form of the strain energy density (Gurtin et al., 2010) is given by

$$\psi = \psi^\nu(J) + \psi^i(\bar{I}_1) = \frac{\hat{\kappa}}{2}(J-1)^2 + \frac{\hat{E}}{6}(\bar{I}_1-3), \quad (3)$$

where $\hat{\kappa}$ and \hat{E} denote the bulk modulus and the initial elastic modulus of the elastomer, respectively. The Cauchy stress \mathbf{T} is found by differentiating ψ with respect to \mathbf{C} , yielding

$$\mathbf{T} = \hat{\kappa}(J-1)\mathbf{1} + \frac{\hat{E}}{3J} \text{dev}(\mathbf{B}^i). \quad (4)$$

where $\mathbf{B}^i = \mathbf{F}^i \cdot \mathbf{F}^{iT}$ and “dev” stands for deviatoric part of 2nd order tensors.

3.2. Cardiac muscle cells

The characteristic energy dissipative process of the cardiomyocyte active contribution can be captured by recently developed physiology-based models, which consider the mechanism of the involuntary contractile behavior of cardiac muscle due to the action potential under calcium flux (Sainte-Marie et al., 2006; Sermesant et al., 2006; Chapelle et al., 2010). However, this approach is mathematically complex, and model parameter identification is challenging. In this article, instead, we take a simple, but effective phenomenological approach, neglecting the energy dissipative process. While recently Böl et al. (2009) developed a phenomenological model for cardiac muscle cells, their formulation neglects the important effect of the pre-stretch that the muscle cells develop as they mature. This paper presents a 3-D phenomenological model that captures the two major features of cardiac muscles: the passive behavior including pre-stretched deformation and their active behavior including systole and diastole.

Kinematics including pre-stretch. Even when resting, muscle cells *in vivo* experience a state of stress due to their pre-stretched conditions. This can be clearly observed from the experimental data reported in Fig. 2B–D and F, showing a non-negligible MTF curvature during diastole. In order to account for such pre-stretched conditions, previous constitutive models introduced an *ad hoc* strain-shift in the stress–strain curve (Blemker et al., 2005; Böl et al., 2009; Calvo et al., 2010) leading to a non-unique material response that depends on the level of pre-stretch of muscle cells. However, such formulation does not capture the non-negligible MTF curvature observed during diastole. Thus, in this paper, a different approach is adopted to model pre-stretch; inspired by the multiplicative decomposition introduced by Kroner (1960) and Lee (1969), the isochoric deformation gradient \mathbf{F}^i in Eq. (2) is decomposed into load-induced, \mathbf{F}^{iL} , and pre-

stretched, \mathbf{F}^{iS} , contributions

$$\mathbf{F}^i = \mathbf{F}^{iL} \cdot \mathbf{F}^{iS}. \quad (5)$$

Here, for the sake of simplicity, the pre-stretch is assumed to be fully developed during cell differentiation and maturation prior to the experiment, and not to be affected by the cell active response. If we also assume that the pre-stretch deformation is incompressible and the cells deform affinely, the pre-stretched contribution to the deformation gradient \mathbf{F}^{iS} is given by

$$\mathbf{F}^{iS} = \mathbf{Q} \Lambda \mathbf{Q}^T, \quad (6)$$

with

$$\Lambda = \hat{\lambda}_S \mathbf{e}_1 \otimes \mathbf{e}_1 + (\hat{\lambda}_S)^{-1/2} (\mathbf{e}_2 \otimes \mathbf{e}_2 + \mathbf{e}_3 \otimes \mathbf{e}_3), \quad (7)$$

$$\mathbf{Q} = \cos \hat{\theta} (\mathbf{e}_1 \otimes \mathbf{e}_1 + \mathbf{e}_2 \otimes \mathbf{e}_2) + \sin \hat{\theta} (-\mathbf{e}_1 \otimes \mathbf{e}_2 + \mathbf{e}_2 \otimes \mathbf{e}_1) + \mathbf{e}_3 \otimes \mathbf{e}_3, \quad (8)$$

where $\hat{\lambda}_S$ is the pre-stretch induced into the cardiac myocytes lying in the x_1 – x_2 plane during maturation (*i.e.*, myogenesis and tissue development) and $\hat{\theta}$ is the angle identifying the cell alignment in the undeformed configuration (see Fig. 1B). The diastole curvatures of the experimental data reported in Fig. 2B–D and F clearly show a deviation in the pre-stretched response of the cells as a result of the diversity in cell conditions. Therefore, we expect the parameter $\hat{\lambda}_S$ not to be uniquely determined, but to be influenced by experimental factors such as, but not limited to, small variations in temperature/humidity, local density variations, local intracellular architecture, and cardiac origin of the cells (left or right ventricle).

Constitutive equations for passive and active behavior. When an isotropic material is reinforced by a family of fibers with direction $\mathbf{a}_0 = \cos \hat{\theta} \mathbf{e}_1 + \sin \hat{\theta} \mathbf{e}_2$ in the reference configuration (Fig. 1B), the isochoric part of the strain energy can be expressed as a function of not only the invariants of \mathbf{C} , but also additional invariants depending on \mathbf{a}_0 . To describe both passive (representing resting status) and active (including systole and diastole) behavior of cardiomyocytes, we specify a decoupled form of free energy as

$$\psi = \psi^\nu(J) + \psi_{iso}^i(\bar{I}_1) + \psi_{ani}^{ip}(\bar{I}_4) + \psi_{ani}^{ia}(\bar{I}_4, q), \quad (9)$$

where $\bar{I}_4 = \mathbf{a}_0 \cdot \mathbf{C}^i \cdot \mathbf{a}_0$ and q is the activation level of cardiac muscle cells. In the proposed model, while ψ^ν and ψ_{iso}^i reflect the volumetric and the isotropic contributions of the intercellular part, respectively, ψ_{ani}^{ip} and ψ_{ani}^{ia} represent the passive and the active contributions of anisotropic effect of the myofibril, respectively. Their detailed forms can be found in Section S2 of the supporting material. By differentiating ψ with respect to \mathbf{C} , the resulting Cauchy stress for the cardiac muscle cells is obtained as

$$\mathbf{T} = \mathbf{T}^\nu + \mathbf{T}_{iso}^i + \mathbf{T}_{ani}^{ip} + \mathbf{T}_{ani}^{ia}, \quad (10)$$

where

$$\mathbf{T}^\nu = \hat{\kappa}(J-1)\mathbf{1}, \quad (11)$$

$$\mathbf{T}_{iso}^i = \frac{\hat{E}_c}{3J} \text{dev}(\mathbf{B}^i), \quad (12)$$

$$\mathbf{T}_{ani}^{ip} = \frac{\hat{E}_p \bar{\lambda}}{\hat{\alpha} J} [e^{\hat{\alpha}(\bar{\lambda}-1)} - 1] \text{dev}(\bar{\mathbf{a}} \otimes \bar{\mathbf{a}}), \quad (13)$$

$$\mathbf{T}_{ani}^{ia} = \begin{cases} \frac{\hat{P}q}{J} \left[1 - \left(\frac{\bar{\lambda} - \hat{\lambda}_0}{1 - \hat{\lambda}_0} \right)^2 \right] \text{dev}(\bar{\mathbf{a}} \otimes \bar{\mathbf{a}}) & \text{if } 1 < \bar{\lambda} < (2\hat{\lambda}_0 - 1), \\ 0 & \text{otherwise.} \end{cases} \quad (14)$$

Table 1
Summary of model parameters and their physical meaning.

PDMS	$\hat{E} = 1.5$ MPa $\hat{\kappa} = 25$ MPa	Initial elastic modulus Initial bulk modulus
<i>Cardiac muscle cell</i>		
Pre-stretched	$\hat{\theta} = 0^\circ, 30^\circ$ $\hat{\lambda}_S \in [1.11, 1.18]$	Angle defining the initial alignment of the cells within the x_1-x_2 plane Pre-stretch developed in the cardiomyocytes during cell maturation
Volumetric	$\hat{\kappa} = 380$ kPa	Initial bulk modulus
Isotropic	$\hat{E}_c = 2.3$ kPa	Initial elastic modulus of intercellular part
Anisotropic	$\hat{E}_p = 21$ kPa	Initial elastic modulus of fiber
Passive	$\hat{\alpha} = 5.5$	Constant related to the slope of stress–strain relation of passive fiber
Anisotropic	$\hat{P} \in [2.8, 21.6]$ kPa	Isometric twitch stress
Active	$\hat{\lambda}_o = 1.24$ $\hat{T} = 0.21$ s	Optimal stretch for the maximum active stress Characteristic time scale for contraction

Table 2
Summary of the model described in Section 3. Note that $g(\tau)$ is an arbitrary time history describing the cell pre-stretch development.

Given at time τ	$\mathbf{F}^{ABQ}(\tau)$: deformation gradient given by ABAQUS
Kinematics	$J(\tau) = \det \mathbf{F}^{ABQ}(\tau)$ $\mathbf{F}^i(\tau) = J(\tau) \mathbf{1}$ $\mathbf{F}^{il}(\tau) = J(\tau)^{-1/3} \mathbf{F}^{ABQ}$ $\Lambda = \hat{\lambda}_S \mathbf{e}_1 \otimes \mathbf{e}_1 + (\hat{\lambda}_S)^{-1/2} (\mathbf{e}_2 \otimes \mathbf{e}_2 + \mathbf{e}_3 \otimes \mathbf{e}_3)$ $\mathbf{Q} = \cos \hat{\theta} (\mathbf{e}_1 \otimes \mathbf{e}_1 + \mathbf{e}_2 \otimes \mathbf{e}_2) + \sin \hat{\theta} (-\mathbf{e}_1 \otimes \mathbf{e}_2 + \mathbf{e}_2 \otimes \mathbf{e}_1) + \mathbf{e}_3 \otimes \mathbf{e}_3$ $\mathbf{F}^{iS}(\tau) = g(\tau) \mathbf{Q} \cdot \Lambda \cdot \mathbf{Q}^T$ $\mathbf{F}(\tau) = \mathbf{F}^v(\tau) \cdot \mathbf{F}^{il}(\tau) \cdot \mathbf{F}^{iS}(\tau)$
Constitutive equation	$\mathbf{a}_0(\tau) = \cos \hat{\theta} \mathbf{e}_1 + \sin \hat{\theta} \mathbf{e}_2$ $\mathbf{C}^i(\tau) = \mathbf{F}^{iT}(\tau) \cdot \mathbf{F}^i(\tau)$ $\bar{\lambda} = \sqrt{\mathbf{a}_0 \cdot \mathbf{C}^i \cdot \mathbf{a}_0}$ $\mathbf{B}^i(\tau) = \mathbf{F}^i(\tau) \cdot \mathbf{F}^{iT}(\tau)$ $\bar{\mathbf{a}}(\tau) = \mathbf{F}^i(\tau) \cdot \mathbf{a}_0 / \bar{\lambda}$ $q(\tau) = \left(\frac{\tau}{\hat{T}}\right)^2 \exp \left[1 - \left(\frac{\tau}{\hat{T}}\right)^2 \right]$ $\mathbf{T}^v(\tau) = \hat{\kappa} (J(\tau) - 1)$ $\mathbf{T}_{iso}^i(\tau) = \frac{\hat{E}_c}{3J(\tau)} \text{dev}(\mathbf{B}^i(\tau))$ $\mathbf{T}_{ani}^{ip}(\tau) = \frac{\hat{E}_p \bar{\lambda}(\tau)}{\hat{\alpha} J(\tau)} [e^{\hat{\alpha}(\bar{\lambda}(\tau)-1)} - 1] \text{dev}(\bar{\mathbf{a}}(\tau) \otimes \bar{\mathbf{a}}(\tau))$ $\mathbf{T}_{ani}^{ip}(\tau) = \begin{cases} \frac{\hat{P} q(\tau)}{J(\tau)} \left[1 - \left(\frac{\bar{\lambda}(\tau) - \hat{\lambda}_o}{1 - \hat{\lambda}_o} \right)^2 \right] \text{dev}(\bar{\mathbf{a}}(\tau) \otimes \bar{\mathbf{a}}(\tau)) & \text{if } 1 < \bar{\lambda}(\tau) < (2\hat{\lambda}_o - 1) \\ 0 & \text{otherwise} \end{cases}$ $\mathbf{T}(\tau) = \mathbf{T}^v(\tau) + \mathbf{T}_{iso}^i(\tau) + \mathbf{T}_{ani}^{ip}(\tau) + \mathbf{T}_{ani}^{ia}(\tau)$

Here, $\bar{\lambda} = \sqrt{\bar{\lambda}_4}$, $\bar{\mathbf{a}} = \mathbf{F}^i \cdot \mathbf{a}_0 / \bar{\lambda}$,

$$q(t) = \left(\frac{t}{\hat{T}}\right)^2 \exp \left[1 - \left(\frac{t}{\hat{T}}\right)^2 \right], \quad (15)$$

and the physical meaning of all the model parameters (*i.e.*, $\hat{\kappa}$, \hat{E}_c , \hat{E}_p , $\hat{\alpha}$, \hat{P} , $\hat{\lambda}_o$, \hat{T}) is summarized in Table 1.

Model implementation. The constitutive model outlined in this section has been implemented into the commercial finite element code ABAQUS/Explicit, using a user-defined subroutine VUMAT, and Table 2 summarizes the model and its implementation. Each FE analysis consists of two steps: the first step simulates the development of pre-stretch into the non-activated cells; in the

second step, the active response of MTFs is simulated under fully pre-stretched conditions.

4. Model parameter identification

In this section, we present the procedure followed to identify the parameters entering in the constitutive model. Additional details are provided in Section S3 of the supporting material.

While the material parameters for the elastomeric substrate ($\hat{E} = 1.5$ MPa, $\hat{\kappa} = 25$ MPa) are provided by the manufacturers, the parameters needed to characterize the cardiac muscle cell response are obtained from the literature and contraction assays

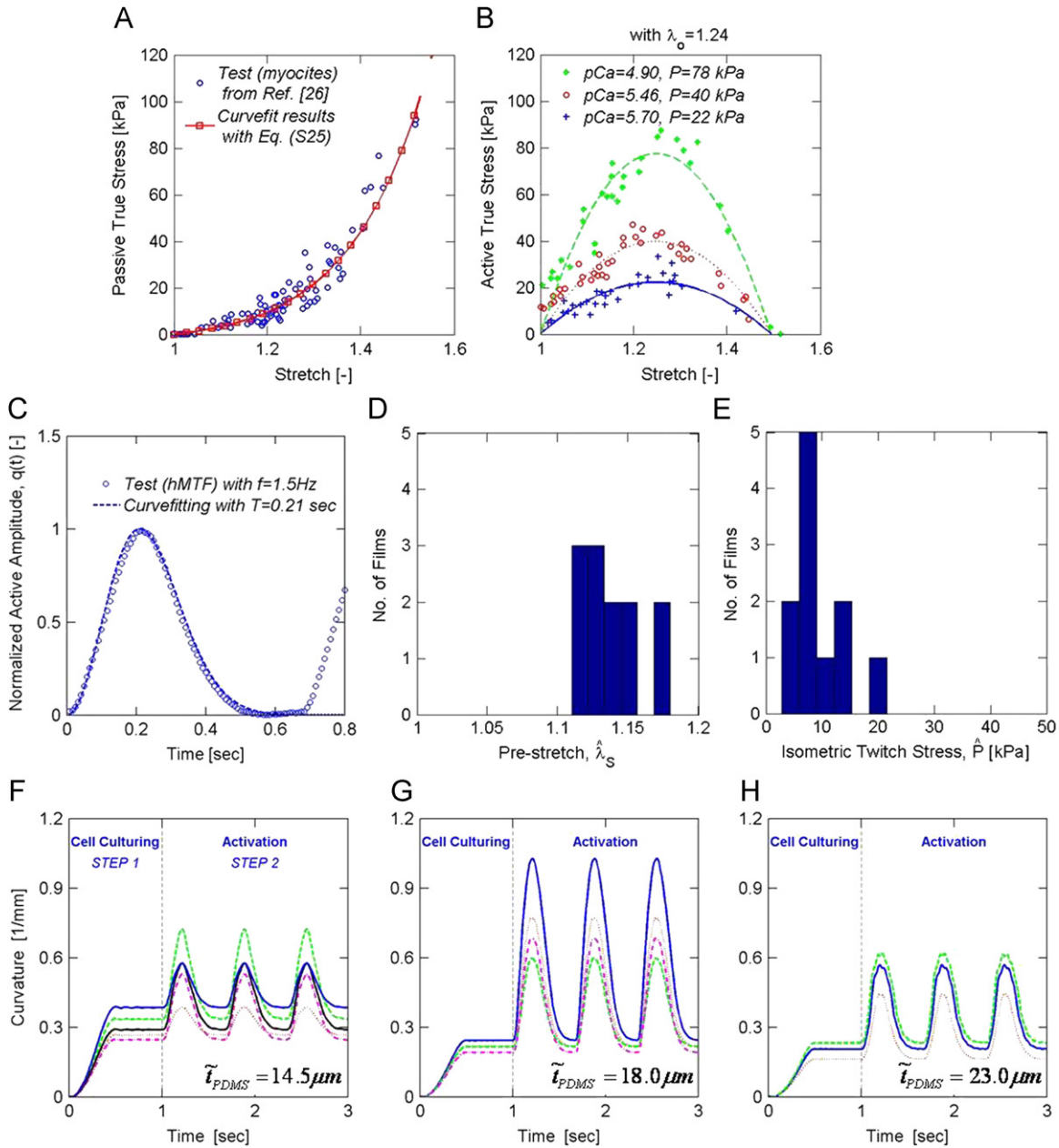


Fig. 3. Model parameter identification from Weiwad et al. (2000) (A and B) and from experiments with length-wise cell alignment (C–H). (A) Tensile behavior of non-activated cells. Blue circular markers denote experimental data and the red line corresponds to Eq. (S21). (B) Isometric twitch stress as a function of calcium concentration ($pCa = -\log_{10}(a_{Ca^{2+}})$). Markers denote experimental data and the lines correspond to Eq. (S21). (C) A typical profile of the active amplitude history from tests performed on MTFs with length-wise cell alignment. Markers denote experimental data, and the line corresponds to $q(t)$ in Eq. (15). (D and E) Range of values identified for $\hat{\lambda}_S$ and \hat{P} . (F–H) Time-curvature plots for MTFs with length-wise cell alignment from FE simulations. Note that one-to-one correspondence between experimental (Fig. 2B–D) and numerical (F–H of this figure) curves. (For interpretation of the references to color in this figure legend, the reader is referred to the web version of this article.)

performed with neonatal rat ventricular myocytes micropatterned on PDMS thin films.

4.1. Parameters identified from the literature

The paper by Weiwad et al. (2000) provides in a single article nearly all the required test results to identify the material parameters entering into the proposed material model. Moreover, all their data are in a good agreement with similar test results for the heart muscle of adult rats (i.e., Granzier and Irving, 1995 and Palmer et al., 1996 for passive behavior and Nishimura et al., 2000 and Palmer et al., 1996 for active behavior). Thus, the test results presented in Weiwad et al.

(2000) are used to identify five material-specific parameters entering into the proposed constitutive model.

From their tensile tests of the non-activated cells (shown in Fig. 3A), we determine three model parameters, i.e., $\hat{E}_c = 21\text{ kPa}$, $\hat{E}_p = 2.3\text{ kPa}$, and $\alpha = 5.5$ by curve-fitting the test results with Eqs. (12) and (13) specialized to uniaxial loading conditions. Moreover, the experimental results obtained for the isometric twitch stress (Fig. 3B) guide us to propose a quadratic form of active stress profile as shown in Eq. (14), and determine $\hat{\lambda}_o = 1.24$. Finally, for the sake of simplicity, we assume that the cardiac muscle is nearly incompressible and its volumetric behavior is determined by the non-activated cell response, resulting in a bulk modulus of $\hat{\kappa} = 380\text{ kPa}$.

4.2. Parameters identified from MTF tests with length-wise cell alignment

Experiments with length-wise cell alignment are used to identify the remaining three model parameters (\hat{P} , $\hat{\lambda}_S$, \hat{T}). While \hat{P} and $\hat{\lambda}_S$ are experimental-conditions-specific, \hat{T} denotes the characteristic time scale of contractile behavior under the stimulating electric pulse. First, $\hat{T} = 0.21$ s is identified by curve-fitting a typical profile of the active amplitude history shown in Fig. 3C with $q(t)$ in Eq. (15).

Secondly, values for both $\hat{\lambda}_S$ and \hat{P} are determined using the experimental data presented in Fig. 2B–D. As in the experiments, MTFs with PDMS substrate of thickness $\tilde{t} = 14.5, 18.0,$ or $23.0 \mu\text{m}$ and cardiac myocytes thickness $\hat{t} = 4 \mu\text{m}$ are modeled and simulated. Since the experiments show a significant variability in the material response for each curvature history shown in Fig. 2B–D, both $\hat{\lambda}_S$ and \hat{P} are determined to achieve the best fit while leaving all the other model parameters unchanged. Thus, a range of values is identified for $\hat{\lambda}_S$ and \hat{P} whose distributions are shown in Fig. 3D and E, respectively. More specifically, we obtain (a) $\hat{\lambda}_S \in [1.11, 1.16]$ and $\hat{P} \in [2.8, 7.3]$ kPa for $\tilde{t} = 14.5 \mu\text{m}$, (b) $\hat{\lambda}_S \in [1.12, 1.14]$ and $\hat{P} \in [9.2, 21.6]$ kPa for $\tilde{t} = 18.0 \mu\text{m}$, and (c) $\hat{\lambda}_S \in [1.16, 1.18]$ and $\hat{P} \in [6.9, 8.5]$ kPa for $\tilde{t} = 23.0 \mu\text{m}$. While a rather small variation in the pre-stretch ranging from $\hat{\lambda}_S = 1.11$ to 1.18 is observed, we find a quite large variation in the isometric twitch stress ranging from $\hat{P} = 2.7$ to 21.6 kPa. Finally, Fig. 3F–H reports the curvature histories of MTFs obtained from FE simulations, clearly showing that the model correctly capture the curvature induced by pre-stretch curvature during cell maturation and the active response.

5. Numerical simulation results

In this section, we first validate the proposed model by simulating MTFs with diagonal cell alignments, and then present a series of parametric studies to investigate the effect of PDMS thickness, isometric twitch stress, and pre-stretch of cells.

5.1. Model validation for MTFs with diagonal cell alignment

In order to validate the proposed model, the identified model parameters listed in Table 1 are used to simulate the behavior of MTFs with diagonal cell alignment. To incorporate the variation of cell conditions observed in MTFs with length-wise cell alignment,

we perform simulations with two extreme sets of parameters: one with $\hat{\lambda}_S = 1.11$ and $\hat{P} = 2.8$ kPa (weakest cell conditions), and the other with $\hat{\lambda}_S = 1.18$ and $\hat{P} = 21.6$ kPa (strongest cell conditions). As shown in Fig. 4A and B, the FE simulations qualitatively capture the experimentally observed behavior (see Fig. 2E). In addition, Fig. 4C clearly shows that all the experimental time–curvature data are bounded by the simulation results obtained using two extreme cell conditions.

5.2. Parametric studies

Since the quantification of stresses within cells is experimentally challenging, inspired by Stoney's approximate plate analysis (Stoney, 1909) various formulations have been proposed to estimate stress from curvature measurements (Atkinson, 1995; Alford et al., 2010). Using the proposed 3-D constitutive model, FEM simulations can provide more accurate predictions for stress and strain distribution. Here, we explore the effect of important parameters within MTF with length-wise cell alignment (e.g., the PDMS thickness, the isometric twitch stress of cells, and the pre-stretch of cells) on the stress history; additional details of the simulations are summarized in Section S4 of the supporting material.

Effect of PDMS thickness. The effect of PDMS thickness on the response of the MTFs is explored by varying \tilde{t} from $13.0 \mu\text{m}$ to $28.0 \mu\text{m}$. The average value of the two cell-condition-dependent parameters is used (i.e., $\hat{\lambda}_S = 1.14$ and $\hat{P} = 9.0$ kPa), while keeping all other parameters unchanged.

Fig. 5A shows the effect of PDMS thickness on the average of maximum principal stress within the cardiac cells, denoted by \bar{S} . In order to obtain \bar{S} , we collect the time history of the maximum principal stress within all the cardiac cell elements, and then calculate the spatial average. It is interesting to observe that the results of the FEM simulations show a negligible effect of the PDMS thickness on the cells stress. To better quantify this behavior, we decompose \bar{S} into the passive contribution (\bar{S}_p) and the active contribution (\bar{S}_a),

$$\bar{S} = \bar{S}_p + \bar{S}_a, \quad (16)$$

and plot their maximum values ($\max(\bar{S}_p)$, $\max(\bar{S}_a)$) separately in Fig. 5B, confirming no effect of the PDMS thickness on the cells stress.

Effect of isometric twitch stress of cells. In the experiments, we observe that the active response of cells largely changes from test to test. In the proposed model, such variation in the cell response

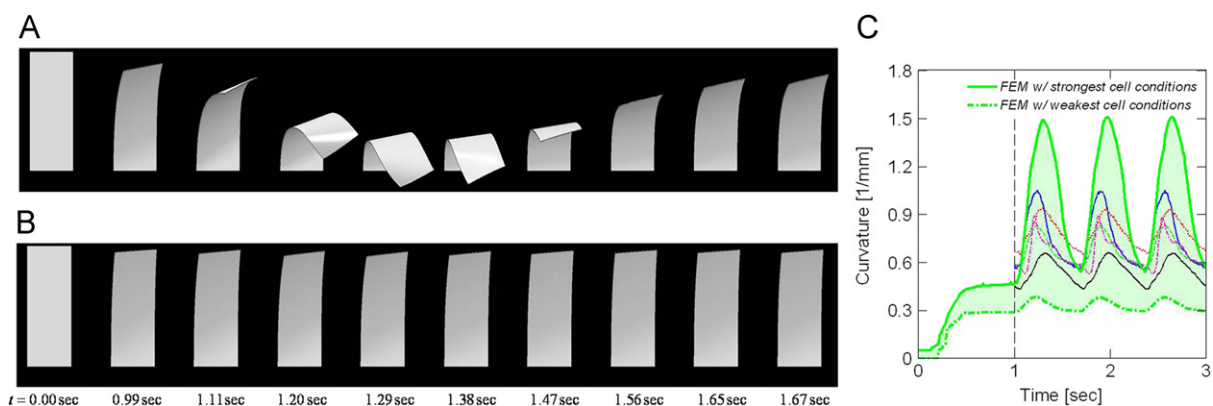


Fig. 4. Contractile behavior of MTF with diagonal cell alignment (PDMS thickness of $14.5 \mu\text{m}$) from FE simulations. (A) Snapshots of FE simulation with strongest cell conditions (i.e., pre-stretch of $\hat{\lambda}_S = 1.18$ and isometric twitch stress of $\hat{P} = 21.6$ kPa). (B) Snapshots of FE simulation with weakest cell conditions (i.e., pre-stretch of $\hat{\lambda}_S = 1.11$ and isometric twitch stress of $\hat{P} = 2.8$ kPa). (C) Comparison of experimental and numerical time–curvature plots. The green shaded region corresponds to the area bounded by simulations with two extreme cell conditions considered in this study. (For interpretation of the references to color in this figure legend, the reader is referred to the web version of this article.)

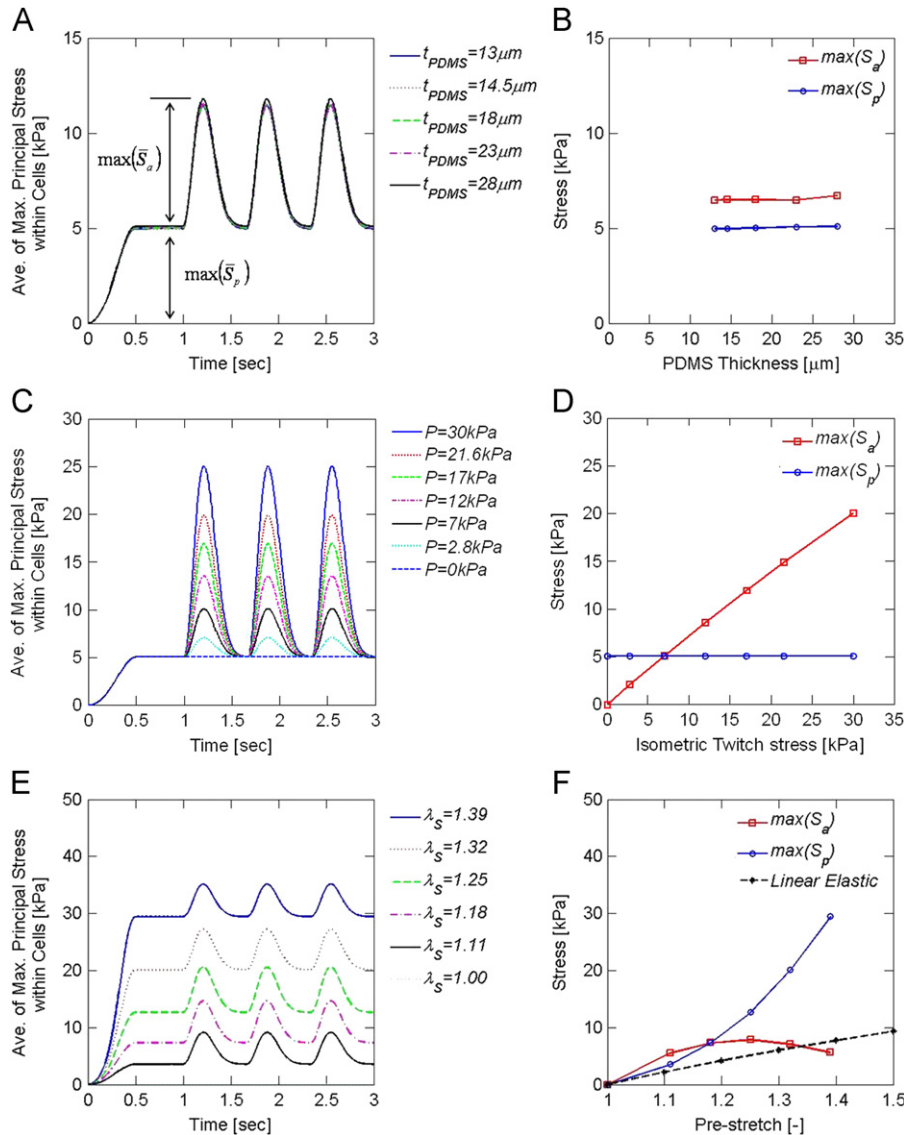


Fig. 5. FE parametric studies: the left column for the averaged histories of maximum principal stress (\bar{S}), and right column for the stress contribution of passive and active response ($\max(S_p)$ and $\max(S_a)$). (A and B) Effect of PDMS thickness, (C and D) effect of isometric twitch stress of cells, (E and F) effect of cell pre-stretch.

can be studied by exploring the value of the isometric twitch stress, \hat{P} . We vary \hat{P} from 0 to 30.0 kPa while keeping all other parameters unchanged, including $\tilde{t} = 18.0 \mu m$ and $\lambda_s = 1.14$. The effect of \hat{P} on the MTF response is reported in Fig. 5C and D, showing that the active stress within the cells increases linearly with the isometric twitch stress, as formulated in Eq. (2).

Effect of cell pre-stretch. It is well known that the pre-stretch within the cells is largely affected by the substrate and the mechanical/chemical stimulus during maturation (Wang et al., 2002; Griffin et al., 2004; Engler et al., 2008). We investigate systematically the effect of pre-stretch (λ_s); the effect of pre-stretch on the cardiomyocyte response is investigated by varying λ_s from 1.00 (*i.e.*, no pre-stretch) to 1.39 while keeping all other parameters unchanged and using $\tilde{t} = 18.0 \mu m$ and $\hat{P} = 9.0$ kPa.

The results are reported in Fig. 5E and F, they indicate that a linear model, $\bar{S}_{linear} = (\bar{E}_c + \bar{E}_p) \ln \lambda_s$, poorly captures the stress distribution within the cells. Moreover, it is interesting to observe that the case with no pre-stretch (*i.e.*, $\lambda_s = 1.00$) results in no stress within the cells. Finally, the simulations also show an exponential form of the stretch-stress relation for the passive fiber response and a quadratic relation for the active fiber

response. Note that because of the quadratic relation between the pre-stretch and the active stress contribution, we observe an optimal pre-stretch value at which a maximum level of active response (*i.e.*, maximum active mobility) is achieved.

6. Discussion and conclusions

6.1. Discussion

In this paper, we investigate through experiments and simulations the response of MTFs with length-wise and diagonal cell alignments. First, we establish a simple procedure based on the measured projection length to quantify the curvature of MTFs with both length-wise and diagonal cell alignments. The proposed method allows, for the first time, quantification of the curvature of MTFs with diagonal cell alignment, suggesting that the procedure can be extended to the analysis of constructs with non-trivial shapes such as swimmers. In order to simulate and predict the observed experimental behavior of MTFs, we propose a 3-D phenomenological constitutive model that captures the passive film deformation

including pre-stretch as well as the active behavior of cardiomyocytes. Inspired by the multiplicative decomposition introduced by Kroner (1960) and Lee (1969), the isochoric deformation gradient is decomposed into load-induced and pre-stretched contributions so that the effect of the pre-stretch can be independently investigated. To simplify the identification of parameters entering in the model, we propose a phenomenological formulation where the cardiomyocyte active contribution is described by an elastic model and all the different aspects of constitutive behaviors are decoupled. Data from literature and experiments conducted on MTFs with length-wise cell alignment are used to identify all the model parameters. Moreover, the variation in mechanical properties observed during experiments is accounted for by identifying a range of values for the induced pre-stretch ($\hat{\lambda}_s$) and the isometric twitch stress (\hat{P}). The resulting formulation captures qualitatively and quantitatively the experimentally observed response of MTFs with diagonal cell alignment. MTFs are characterized by a very complicated chemo-mechanical behavior. To capture the salient features of their response with a sufficiently simple formulation, several assumptions need to be made: here, the energy dissipating mechanism is neglected and a decoupled form of free energy is adopted.

Recently proposed physiology-based constitutive models consider the mechanism of the involuntary contractile behavior of cardiac muscle due to the action potential under calcium flux (Sainte-Marie et al., 2006; Sermesant et al., 2006; Chapelle et al., 2010). These formulations capture the characteristic energy dissipative process of the cardiomyocyte active contribution and satisfy the thermodynamics laws. However, these models are mathematically complex and lead to sophisticated procedures for the identification of the model parameters (Sermesant et al., 2006), making unrealistic the use of such models as design tools for MTF actuators. Instead, we take a simple, but effective phenomenological approach in the spirit of Blemker et al. (2005) and Böl et al. (2009), where the energy dissipative behavior of the active contribution is neglected. To describe the active response of cardiomyocytes, an elastic model is adopted and a scalar internal variable (q in Eq. (15)) is introduced, leading to a formulation that does not satisfy the free energy imbalance conditions.

Several theories for metal plasticity (Brown et al., 1989), approximately incompressible elastic materials (Anand, 1996), and fiber-reinforced composite (Spencer, 1984) are based on a separable form of free energy (the so-called *separability hypothesis* Gurtin et al., 2010) and consider separately the contributions of plastic, volumetric and anisotropic deformation. This formulation provides an effective way to incorporate various aspect of the complex material behavior into a relatively simple model. Inspired by this approach, we decouple all the aspects of the muscle response (see Eq. (9)) although there is no experimental evidence for such assumption. However, this formulation leads to a substantially simplified procedure for the identification of the model parameters; most of them can be identified from literature, and only a few need to be identified from reference experiments.

6.2. Conclusions

We present a 3-D phenomenological constitutive model that captures the passive film deformation including pre-stretch during cell maturation as well as the active behavior of the cardiac muscle cells. While a range of values is identified for two model parameters (induced pre-stretch $\hat{\lambda}$ and isometric twitch stress \hat{P}) to account for the variation in mechanical properties observed in experiments, all other model parameters are obtained from the literature. The proposed model is implemented within a FE framework and used to simulate the experimental results of diastolic and systolic conformations in a muscular thin film. With the identified model parameters, the proposed model

qualitatively captured the behavior of MTFs with diagonal cell alignment, and all the experimental time–curvature data are bounded by the numerical results obtained using two extreme cell conditions.

The proposed constitutive model can be immediately extended to the analysis of constructs with non-trivial 3-D initial geometries. This will greatly aid in the engineering of soft muscle-powered robots, but it will require a computationally efficient implementation of the model and the use of shell elements within the FE framework. Furthermore, the model has the potential to take into account fluid–structure interactions, opening avenues for the design of swimming constructs, actuators, and micro-fluidic devices.

Conflict of interest statement

The authors report that no conflicts of interest, financial or otherwise, influenced this work.

Acknowledgements

This work has been supported by the Harvard Materials Research Science and Engineering Center under NSF award number DMR-0820484 (KB), DMR-0213805 (KKP), and NIH grant 1 R01 HL079126 (KKP). We are grateful to the Center of Nanoscale Systems at Harvard University for the use of their cleanroom facilities, to Alexander P. Nesmith for developing the brick patterned stamps, and to Harvard SEAS Academic Computing for their support.

Appendix A. Supplementary data

Supplementary data associated with this article can be found in the online version at doi:10.1016/j.jbiomech.2011.11.024.

References

- Alford, P.W., Feinberg, A.W., Sheehy, S.P., Parker, K.K., 2010. Biohybrid thin films for measuring contractility in engineered cardiovascular muscle. *Biomaterials* 31 (13), 3613–3621.
- Anand, L., 1996. A constitutive model for compressible elastomeric solids. *Computational Mechanics* 18 (5), 339–355.
- Atkinson, A., 1995. *British Ceramic Proceedings* 54 (1).
- Blemker, S.S., Pinsky, P.M., Delp, S.L., 2005. A 3D model of muscle reveals the causes of nonuniform strains in the biceps brachii. *Journal of Biomechanics* 38, 657–665.
- Böl, M., Reese, S., 2008. Micromechanical modelling of skeletal muscles based on the finite element method. *Computer Methods in Biomechanics and Biomedical Engineering* 11, 489–504.
- Böl, M., Reese, S., Parker, K.K., Kuhl, E., 2009. Computational modeling of muscular thin film for cardiac repair. *Computational Mechanics* 43, 535–544.
- Brown, S.B., Kim, K.H., Anand, L., 1989. An internal variable constitutive model for hot-working of metals. *International Journal of Plasticity* 5 (2), 95–130.
- Calvo, B., Ramirez, A., Alonso, A., Grasa, J., Soteras, F., Osta, R., Munoz, M.J., 2010. Passive nonlinear elastic behaviour of skeletal muscle: experimental results and model formulation. *Journal of Biomechanics* 43, 318–325.
- Chapelle, D., Gerbeau, J.F., Sainte-Marie, J., Vignon-Clementel, I.E., 2010. A poroelastic model valid in large strains with applications to perfusion in cardiac modeling. *Computational Mechanics* 46, 91–101.
- Engler, A.J., Carag-Krieger, C., Johnson, C.P., Raab, M., Tang, H.-Y., Speicher, D.W., Sanger, J.W., Sanger, J.M., Discher, D.E., 2008. Embryonic cardiomyocytes beat best on a matrix with heart-like elasticity: scar-like rigidity inhibits beating. *Journal of Cell Science* 121, 3794–3802.
- Feinberg, A.W., Feigel, A., Shevkoplyas, S.S., Sheehy, S., Whitesides, G.M., Parker, K.K., 2007. Muscular thin films for building actuators and powering devices. *Science* 317 (5843), 1366–1370.
- Granzier, H.L., Irving, T.C., 1995. Passive tension in cardiac muscle: contribution of collagen, titin, microtubules, and intermediate filaments. *Biophysical Journal* 68, 1027–1044.
- Griffin, M.A., Engler, A.J., Barber, T.A., Healy, K.E., Sweeney, H.L., 2004. Patterning, prestress, and peeling dynamics of myocytes. *Biophysical Journal* 86, 1209–1222.

- Gurtin, M.E., Fried, E., Anand, L., 2010. *The Mechanics and Thermodynamics of Continua*. Cambridge University Press, New York.
- Kroner, E., 1960. Allgemeine kontinuums theorie der versetzungen und eigenspannungen. *Archive for Rational Mechanics and Analysis* 4, 273–334.
- Lee, E.H., 1969. Elastic-plastic deformation at finite strains. *Journal of Applied Mechanics* 36, 1.
- Nishimura, S., Yasuda, S., Katoh, M., Yamada, K.P., Yamashita, H., Saeki, Y., Sunagawa, K., Nagai, R., Hisada, T., Sugiura, S., 2000. Single cell mechanics of rat cardiomyocytes under isometric unloaded and physiologically loaded conditions. *AJP—Heart and Circulatory Physiology* 287, H196–H202.
- Palmer, R.E., Brady, A.J., Roos, K.P., 1996. Mechanical measurements from isolated cardiac myocytes using a pipette attachment system. *AJP—Cell Physiology* 270, C697–C704.
- Place, E.S., Evans, N.D., Stevens, M.M., 2009. Complexity in biomaterials for tissue engineering. *Nature Materials* 8 (6), 457–470.
- Sainte-Marie, J., Chapelle, D., Cimiran, R., Sorine, M., 2006. Modeling and estimation of the cardiac electromechanical activity. *Computers and Structures* 84, 1743–1759.
- Sermesant, M., Moireau, P., Camara, O., Sainte-Marie, J., Andriantsimavona, R., Cimiran, R., Hill, D.L.G., Chapelle, D., Razavi, R., 2006. Cardiac function estimation from MRI using a heart model and data assimilation: advances and difficulties. *Medical Image Analysis* 10, 642–656.
- Spencer, A.J.M., 1984. *Continuum Theory of the Mechanics of Fibre-reinforced Composites*. Springer-Verlag, Wien-New York.
- Stoney, G.G., 1909. The tension of metallic films deposited by electrolysis. *Proceedings of the Royal Society of London A* 82, 172–175.
- Wang, N., Tolic-Norrelykke, I.M., Chen, J., Mijailovich, S.M., Butler, J.P., Fredberg, J.J., Stamenovic, D., 2002. Cell prestress. I. Stiffness and prestress are closely associated in adherent contractile cells. *AJP—Cell Physiology* 282, C606–C616.
- Weiss, J.A., Marker, B.N., Govindjee, S., 1996. Finite element implementation of incompressible, transversely isotropic hyperelasticity. *Computer Methods in Applied Mechanics and Engineering* 135, 107–128.
- Weiwad, W.K.K., Linke, W.A., Wussling, M.H.P., 2000. Sarcomere length-tension relationship of rat cardiac myocytes at lengths greater than optimum. *Journal of Molecular and Cellular Cardiology* 32, 247–259.